Gr-114

LA-7221-MS
Informal Report

132
5-31-78

UC-28
Issued: May 1978

Transient Thermal Stress Analysis of a Proposed Pion Production Target

Lloyd O. Lindquist
Edward C. Scarbrough*

*Summer Graduate Student. New Mexico State University, Las Cruces, NM 88001.

los alamos
scientific laboratory
of the University of California
LOS ALAMOS, NEW MEXICO 87545

An Affirmative Action/Equal Opportunity Employer

UNITED STATES
DEPARTMENT OF ENERGY
CONTRACT W-7405-ENG. 36

TRANSIENT THERMAL STRESS ANALYSIS OF A PROPOSED PION PRODUCTION TARGET

by

Lloyd O. Lindquist and Edward C. Scarbrough

ABSTRACT

We present the results of a transient temperature and stress analysis of a proposed LAMPF proton target. The target configuration, suitable for the LAMPF A-1, A-2, or A-5 pion production sites (800-MeV protons, 1-mA average current), is composed of pyrolytic graphite and is cooled by flowing water.

Special attention is paid to the pulsed nature of the proton beam (6% duty). The computer code TSAAS is used to develop a temperature and stress history of the target during the first five beam pulses and the final, steady-state temperature distribution.

The results of this analysis indicate that a conduction-cooled pyrolytic graphite target of the type shown in this report will be suitable as a LAMPF pion production target at a beam current of 1 mA.

I. INTRODUCTION

In 1979, the Clinton P. Anderson Meson Physics Facility (LAMPF) plans to operate the accelerator at design current (800-MeV protons, average current of 1 mA). Calculations by Lloyd O. Lindquist, Philip Varghese,[1] and Robert J. Macek[2] show that the nonspinning, radiatively cooled graphite targets at the A-1 and A-2 pion production areas will reach hot-spot temperatures of 2300 K at an average beam current of ~0.5 mA. The targets evaporate at an unacceptable rate at this temperature. (Figure 1 is the evaporation-rate vs temperature curve for graphite.) A study was initiated to develop new target-cooling configurations which will meet the requirements of the milliampere beam conditions.

A previous report[3] presented the results of a steady-state thermal stress analysis of a proposed target configuration suitable for the LAMPF A-1, A-2, or A-5 pion production areas. The target (Fig. 2) was analyzed using the computer code TSAAS[4] for maximum temperatures and stresses to be experienced under maximum LAMPF beam current (1 mA). The target modeled was pyrolytic graphite with fixed temperature boundary conditions simulating the effect of cooling at the boundaries. The results of this analysis indicated that the pyrolytic graphite target should withstand a constant heat deposition of 40 kW, the average power deposition of the 800-MeV protons in an 8-cm-thick pyrolytic graphite target at a current of 1 mA, nonpulsed.

Since the beam current is not constant in time, but is pulsed, the steady-state analysis neglects transient temperatures and stresses which may adversely affect the viability of the target. For this

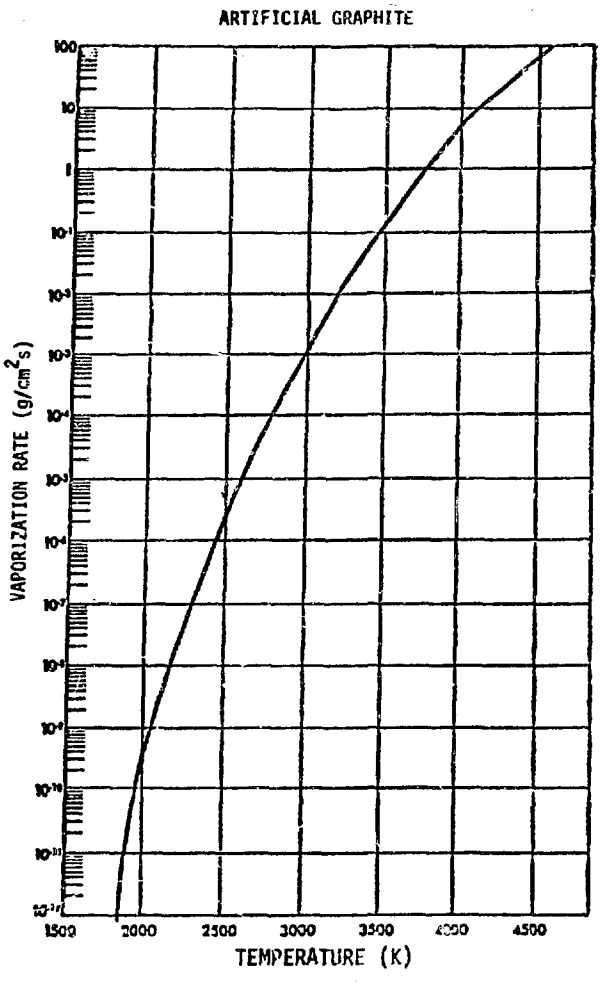

Fig. 1.
Evaporation-rate curve for pyrolytic graphite.

reason, this follow-up analysis was performed to determine the effect of the beam macropulse structure (500-μs burst every 8$^1/_3$ ms, see Fig. 3) on the proposed target.* The analysis was carried out using the computer code TSAAS. Results indicate that the pyrolytic graphite target should withstand the power deposition calculated for LAMPF design current.

*Each macropulse has a microstructure consisting of a 0.25-ns burst every 5 ns. Due to the response time of the material, this was neglected.

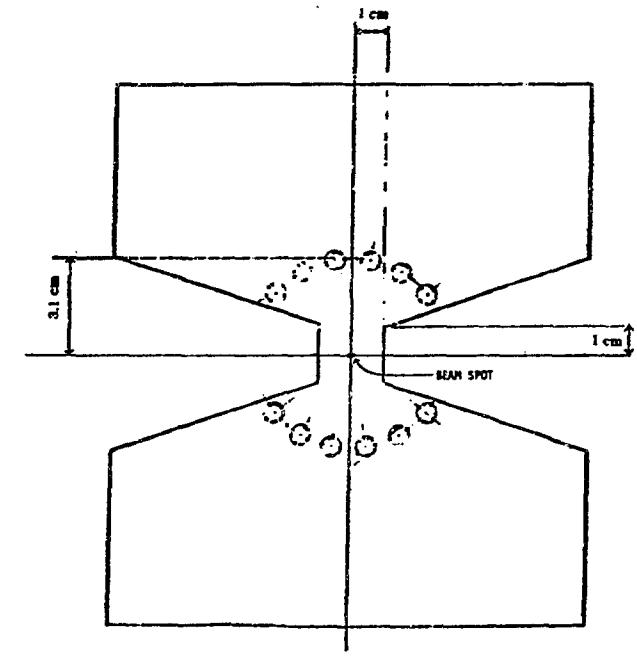

Fig. 2.
Water-cooled pyrolytic graphite target.

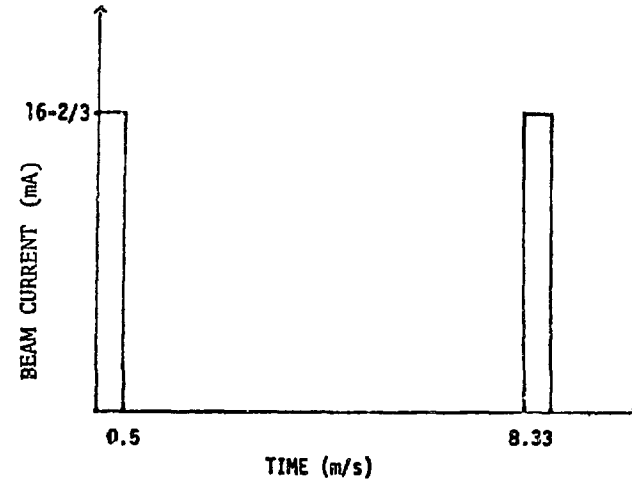

Fig. 3.
Pulse height and width of proton beam current.

II. PYROLYTIC GRAPHITE

The target configuration analyzed is shown in Fig. 2. It is composed of pyrolytic graphite cooled by water flowing through copper tubes bonded to the graphite. The I-beam structure was chosen for several reasons. The I-beam shape allows the target to be inserted or removed without undesirable material (such as copper or water) interacting with the proton beam. The shape provides a minimum of interference with the experimental channels; there is no excess material between the place where pions are born in the proton target and the experimental channel that will utilize the pions. Multiple scattering and loss in energy are minimized. Finally, the circular arc of cooling tubes provides an isothermal heat-transfer interface to eliminate heat flux gradients at the cooling interface.

The geometry of Fig. 2 is unnecessarily complicated for use in the TSAAS analysis. Figure 4 is an excellent thermal representation; it preserves the important features of Fig. 2 while having a relatively simple geometry. A quarter section of the target is analyzed, since the proton beam axis lies at the intersection of the lines of symmetry. There is no net heat-transfer across the lines of symmetry.* The approximations made in using Fig. 4 are given below.

The structural, or "a-b," planes of the pyrolytic graphite are oriented perpendicular to the beam axis. This leads to a relatively short thermal path between the hot spot and the cooling interface.** Hence, the arc of tubes can be thermally approximated by a circular boundary of constant temperature, where one assumes that water flows across the entire boundary. In addition, the change in energy loss of the protons along the thickness of the target is about 1% (see Sec. IV). Assuming uniform power deposition in the proton target, there will be no temperature gradient along the beam axis. The thermal stresses between planes should be minimal and are neglected.†

*Unless otherwise stated, material boundaries bordering on unspecified media are considered perfect insulators.

**The thermal conductivity of pyrolytic graphite in the a-b plane is better than that of copper.

†In a planar analysis, the target is assumed to be of unit thickness.

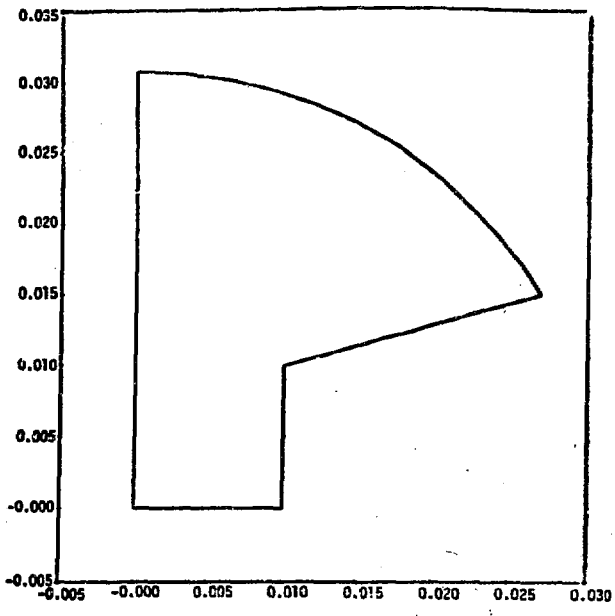

Fig. 4.
Computer model of target geometry.

III. TSAAS

TSAAS is a computer code capable of performing transient or steady-state thermal stress analysis of axisymmetric solids. The version we used, P-TSAAS, analyzes planar materials of arbitrary shape.

The chief inputs to the code are the target geometry, a logical map of the target, material properties, and boundary conditions. The code then approximates the continuous material by a set of discrete nodes, the number and general location of the nodes being specified by the coordinates of the line segments defining the logical map. The temperatures and stresses are computed numerically at the nodes.

The mesh (map of nodes) that was used for this analysis is shown in Fig. 5. This gave a large number of nodes in the region of interest (near the beam spot) while keeping the total number small enough to avoid excessive computational time.

IV. BEAM HEATING

One of the options available with TSAAS is to assign an internal heat-generation rate to a block of

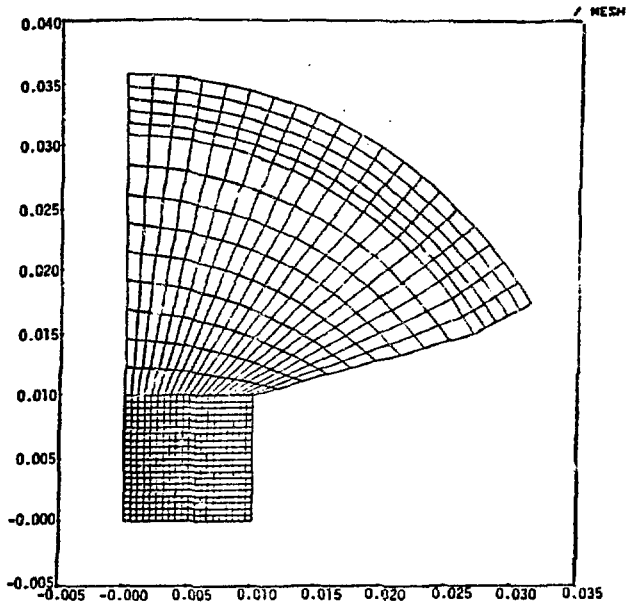

Fig. 5.
Target mesh.

nodes. The rate has units of power per unit mass and is homogeneous over the designated block. We were able to simulate the Gaussian nature of the beam current density (and, thus, the Gaussian nature of the beam heating) by assigning to various blocks of nodes internal heat-generation rates which varied in an approximately Gaussian fashion.

Assuming that the beam current distribution is Gaussian in x and y (perpendicular to the beam axis) and constant in z (parallel to the beam axis), an equation for the power loss distribution in pyrolytic graphite is

$$\frac{dP}{dZ} = \frac{\frac{dE}{dz} \times I}{2\pi\sigma_x\sigma_y} \; e^{-\frac{1}{2}\left(\frac{x^2}{\sigma_x^2} + \frac{y^2}{\sigma_y^2}\right)} , \quad (1)$$

where dE/dz is the energy loss per unit distance in graphite, I is the beam current, x and y are the displacements from the beam center, and σ_x and σ_y are the standard deviations of the beam current density in x and y. The energy loss per unit distance of an 800-MeV proton in pyrolytic graphite (ρ = 2.2 g/cm^3) is

$$\frac{dE}{dz} = \frac{2.1 \text{ MeV-cm}^2}{\text{g = proton}} \times 2.2 \frac{\text{g}}{\text{cm}^3} = 4.62 \frac{\text{MeV}}{\text{cm-proton}} . \quad (2)$$

Assuming an average beam current of 1 mA, we have an instantaneous pulse current of

$$I = 10^{-3} \text{ C/s} \div (120 \text{ pulses/s} \times 500 \; \mu\text{s/pulse})$$

$$= 1.667 \times 10^{-2} \text{ C/s} = 1.667 \times 10^{-2} \text{ C/s} \div 1.6 \times 10^{-19} \text{ proton/C}$$

$$= 1.04 \times 10^{17} \text{ proton/s} .$$

Thus, the total power loss per centimeter is

$$dP/dz = dE/dz \times I = 4.62 \text{ MeV/cm-p} \times 1.04 \times 10^{17} \text{ p/s} = 4.7 \times 10^{17} \text{ MeV/s-cm} \times 1.6 \times 10^{-10} \text{ J/MeV} = 7.7 \times 10^{4} \text{ W/cm} , \quad (3)$$

and the total power deposited in a given region of an 8-cm-thick target ($0 \geq z \geq 0.08$ m, $y_o \geq y \geq y_1$, $x_o \geq x \geq x_1$) is

$$P = \int_{x_o}^{x_1} \int_{y_o}^{y_1} \int_{0}^{.08} \frac{dE}{dz} \times I \frac{e^{-\frac{1}{2}\left(\frac{x^2}{\sigma_x^2} + \frac{y^2}{\sigma_y^2}\right)}}{2\pi\sigma_x\sigma_y} dx\,dy\,dz$$

$$= 6.16 \times 10^{5} \; W \int_{x_o}^{x_1} \int_{y_o}^{y_1} \frac{e^{-\frac{1}{2}\left(\frac{x^2}{\sigma_x^2} + \frac{y^2}{\sigma_y^2}\right)}}{2\pi\sigma_x\sigma_y} dx\,dy \quad (4)$$

during the pulse.

This estimate is slightly low as dE/dz increases with decreasing proton energy. The increase is 0.066 MeV/cm over the range of 40 MeV (4.62 MeV/cm × 8 cm, near 800 MeV). This is roughly 1% of the energy loss and is accounted for by rounding up to 6.8×10^5 W.

Since 99.48% of the beam is contained within the region ($3\sigma_x \leq x \leq 3\sigma_x$, $3\sigma_y \leq y \leq 3\sigma_y$), the amount of power dissipated outside this region was neglected. The region of power deposition in the quarter section analyzed was divided into nine sections, each of dimensions σ_x by σ_y by 0.008 m.

The minimum beam parameters given for the LAMPF proton beam are

$$2\sigma_x = 3 \text{ mm}$$

$$2\sigma_y = 1 \text{ mm}$$

on Line A. These quantities are the results of measurements of current LAMPF beam profiles near Target Cell A-1, the smallest available profiles on Line A. The minimum beam profile should produce the highest temperatures and stresses in the target material. The results obtained using these parameters thus constitute an upper limit for temperatures and stresses to be encountered in any Line A target position (A-1, A-2, ..., A-6). Table I gives the total power loss per unit mass in each of the nine heated regions using the above values of σ_x and σ_y.

V. ANALYSIS OF FIRST FIVE PULSES

The times at which the stresses were considered to be most critical were the first few pulses and the n + 1 pulse, where n is a large number (the steady-state temperature distribution). The first pulses were considered critical because the temperature would rise by hundreds of degrees at the hot spot, while the surrounding material, due to the response time of the material, would remain at the same temperature. Since pyrolytic graphite has increasing strength with increasing temperature, the target was thought more likely to fail during the first few pulses. The steady state was considered important because the temperatures would reach a maximum in the steady state.

TSAAS is not capable of treating the internal heat-generation rate as a function of time. To get the effect of the pulse structure, the program was

TABLE I

POWER PER UNIT MASS IN NINE HEATED REGIONS

P = Power dissipated in each region

$$= 6.16 \times 10^5 \text{ W} \int_{x_o}^{x_1} \int_{y_o}^{y_1} \frac{e^{-\frac{1}{2}\left(\frac{x^2}{\sigma_x^2} + \frac{y^2}{\sigma_y^2}\right)}}{2\pi\sigma_x\sigma_y} dx\,dy .$$

Region	x_o	x_1	y_o	y_1	Power per Unit Mass	(MW/kg)
1	0	σ_x	0	σ_y	6.0×10^8	600.0
2	σ_x	σ_x	0	σ_y	2.38×10^8	238.0
3	$2\sigma_x$	σ_x	0	σ_y	4.08×10^7	40.8
4	0	$2\sigma_x$	σ_y	σ_y	2.38×10^8	238.0
5	σ_x	$2\sigma_x$	σ_y	σ_y	9.56×10^7	95.6
6	$2\sigma_x$	$2\sigma_x$	σ_y	σ_y	1.6×10^7	16.0
7	0	$3\sigma_x$	$2\sigma_y$	$2\sigma_y$	4.08×10^7	40.8
8	σ_x	$3\sigma_x$	$2\sigma_y$	$2\sigma_y$	1.6×10^7	16.0
9	$2\sigma_x$	$3\sigma_y$	$2\sigma_y$	$2\sigma_y$	2.55×10^8	2.55

run using the Gaussian internal heat-generation rate of the previous section to determine the thermal stresses during the first 500 μs. At 500 μs, the nodal point temperatures were stored in a permanent disk file. The program was then run without the internal heat-generation rate, initializing the nodal point temperatures to those in the file. After 7.833 ms of heat transfer (the time between pulses), the temperatures from this calculation were stored in a file. In this way, we were able to introduce the necessary time dependence into our analysis and build a temperature history of the nodes to the total number of pulses desired.

The material properties used in this calculation are given in Table II-A. Given a maximum of six input values, TSAAS will generate a piecewise linear function which describes a specified material property as a function of temperature. As was shown in the previous report,[3] the only material properties which vary significantly over the temperature ranges considered (350-800 K) are the thermal conductivity and the heat capacity. Their values and the temperatures at which these values were taken are shown in Table II-B.

Using the time-dependent Gaussian heating and the material properties given above, we calculated the maximum temperatures and stresses for the first 8.333 ms; the results are shown in Figs. 6 and 7. In all cases calculated, the maximum temperatures and stresses occurred at the end of the pulse. Figures 8 and 9 show the maximum temperatures and stresses at the end of each of the first five pulses.*

The temperatures and stresses calculated during the first five pulses are well within the published tolerances of pyrolytic graphite. There are no anomalous increases in stress during any of these five pulses, and the curves rise in a well-behaved fashion toward some steady-state condition.

VI. STEADY-STATE OSCILLATION OF TEMPERATURES AND STRESSES

Rather than repeat the above calculations n times to reach a steady state (where n appears to be a large number), the nodal point temperatures were initialized to the steady-state temperatures calculated in the previous report. Using this initial temperature distribution, the calculations of the previous section were repeated. After five additional pulses, the calculated hot-spot temperature oscillated between a constant maximum and a constant minimum (±1 K). Figures 10 and 11 show the

*The maximum temperatures and stresses experienced by the material always occur at the beam axis.

TABLE II-A

TEMPERATURE-INDEPENDENT PROPERTIES OF PYROLYTIC GRAPHITE IN THE "A" DIRECTION

Property	Value
Density (kg/m³)	2.2×10^3
Elastic Modulus (Pa)	3.1×10^{10}
Poisson's Ratio	0.24
Coefficient of Thermal Expansion (K^{-1})	2.1×10^{-6}
Ratio of Plastic to Elastic Modulus	1
Ultimate Tensile Strength[a] (Pa)	10^8
Ultimate Compressive Strength (Pa)	10^8
Sublimation Point (K)	3970

[a]The ultimate tensile strength of pyrolytic graphite does not increase significantly until about 2000 K.

TABLE II-B

TEMPERATURE-DEPENDENT PROPERTIES OF PYROLYTIC GRAPHITE

Property	Temperature	Value
Thermal Conductivity (W/m K)	350	1690
	400	1460
	500	1130
	600	930
	700	790
	800	680
Heat Capacity (J/kg K)	350	882
	400	990
	500	1192
	600	1368
	700	1489
	800	1580

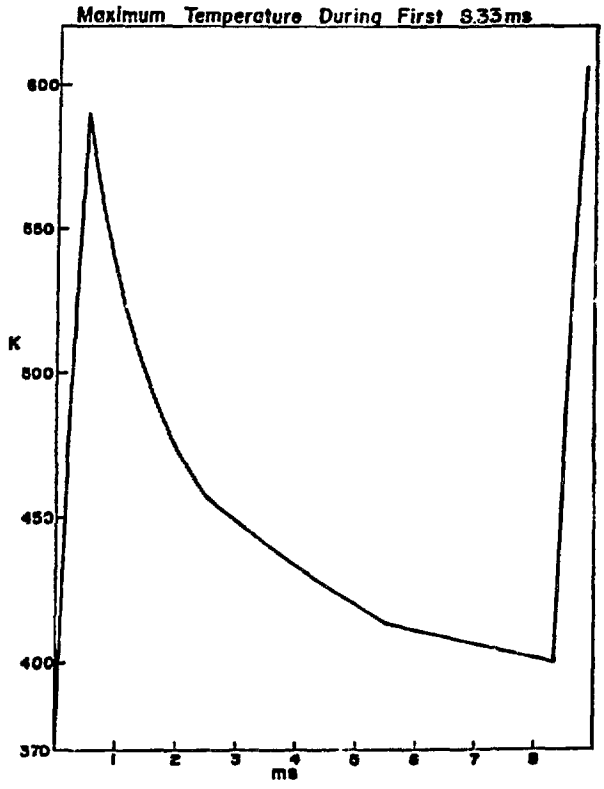

Fig. 6.
Maximum (hot-spot) temperature during first pulse.

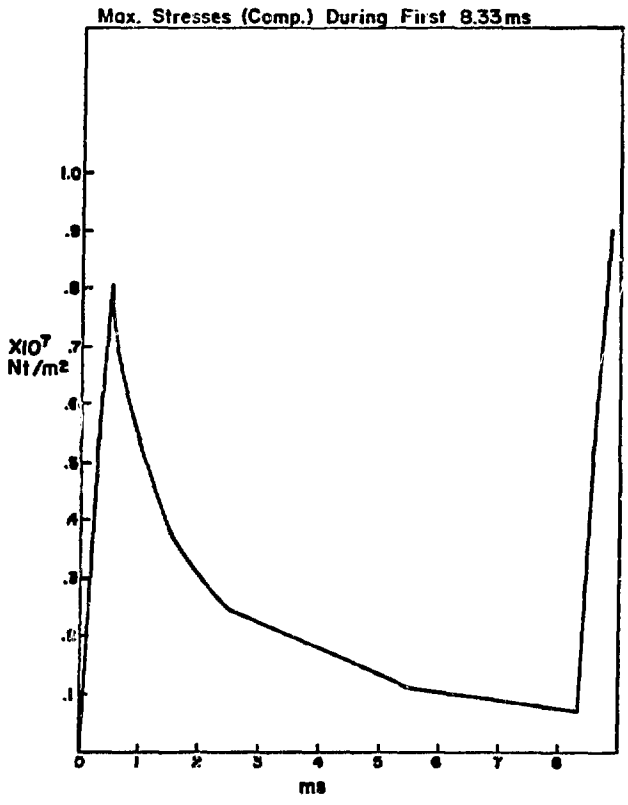

Fig. 7.
Maximum stress (compressional) during the first pulse.

maximum temperatures and stresses over the sixth pulse and the beginning of the seventh.* The maximum temperature reached in this steady-state oscillation is 827 K and the maximum stress is 11.4 MPa (in compression). The thermal response time of the target is such that the steady-state calculations of the previous report are an accurate description of the temperature distribution for the remainder of the target volume not irradiated by the proton beam. As Figs. 12 and 13 show, the stresses are slightly different. Rapid expansion of the material near the beam spot leads to added stresses in the region at which the target fans out. The largest of these stresses are, however, almost three times less than the beam-spot stresses. The maximum stresses in the beam-spot area are 11% of the published values for the ultimate compressive strength of pyrolytic graphite.

VII. SUMMARY

A proposed target configuration was analyzed for maximum temperatures and stresses to be experienced under LAMPF's design current. This analysis has focused on the first five pulses and the steady state as points of most probable material failure. Results obtained using the computer code TSAAS indicate that the maximum temperatures are well below the temperature at which surface evaporation becomes important (Fig. 1). The maximum stresses computed from this temperature distribution are 11% of the compressive strength of pyrolytic

*Inspection of Figs. 6 and 10 show a temperature difference between the beginning and end of the pulse of 227 and 173 K, respectively. This is a decrease in temperature gain of 24%. Inspection of the average heat capacities, however, shows a 21% gain in heat capacity from the average temperature in Fig. 6 to the average temperature in Fig. 10. Therefore, this decrease in temperature gain is to be expected.

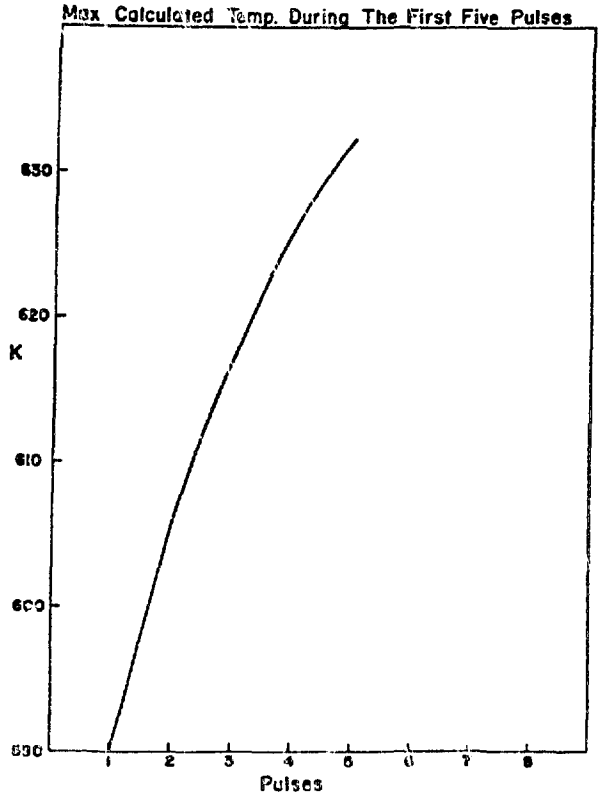

Fig. 8.
Maximum target temperatures at the end of the first five pulses.

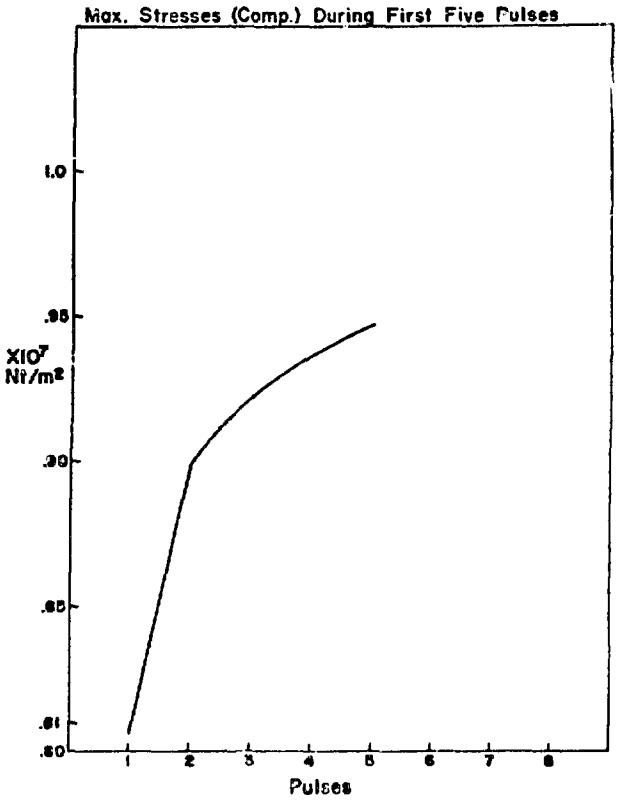

Fig. 9.
Maximum target stresses (compressional) during the first five pulses.

graphite. This analysis and the previous steady-state analysis indicate that a conduction-cooled pyrolytic graphite target of the geometry indicated in this report will be suitable as a LAMPF pion production target.

ACKNOWLEDGMENT

The authors wish to express their gratitude to R. V. Browning for his invaluable aid in the use of TSAAS.

REFERENCES

1. P. Varghese, Los Alamos Scientific Laboratory, private communication, 1976.
2. A. Aldridge and R. J. Macek, Los Alamos Scientific Laboratory, private communication, 1976.
3. L. O. Lindquist and E. C. Scarbrough, "Steady-State Temperature and Stress Distributions of a Proposed LAMPF Pyrolytic Graphite Pion Production Target," Los Alamos Scientific Laboratory report *LA-6936-MS (November* 1977).
4. R. V. Browning, D. G. Miller, and C. A. Anderson, "TSAAS: Finite Element Thermal and Stress Analysis of Axisymmetric Solids with Orthotropic Temperature-Dependent Material Properties," Los Alamos Scientific Laboratory report LA-5599-MS (May 1974).

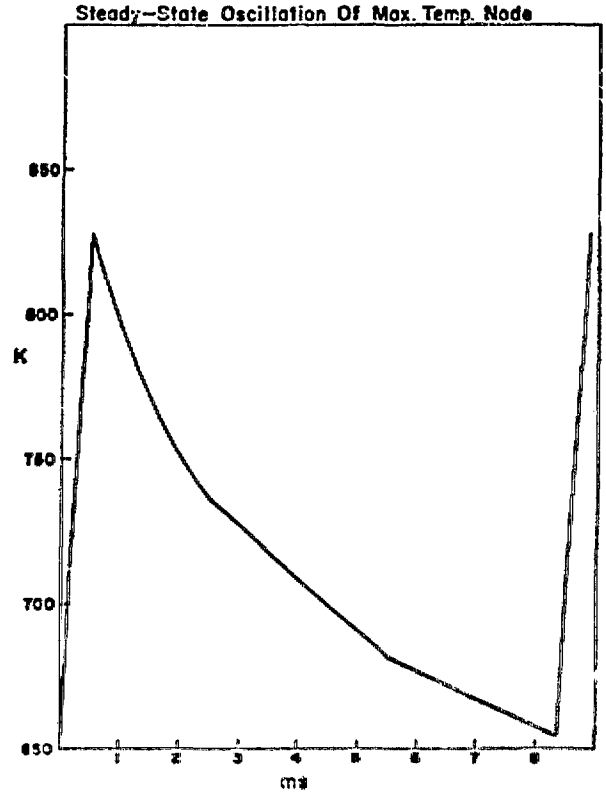

Fig. 10.
Maximum temperature during the n + 1 pulse (n → ∞).

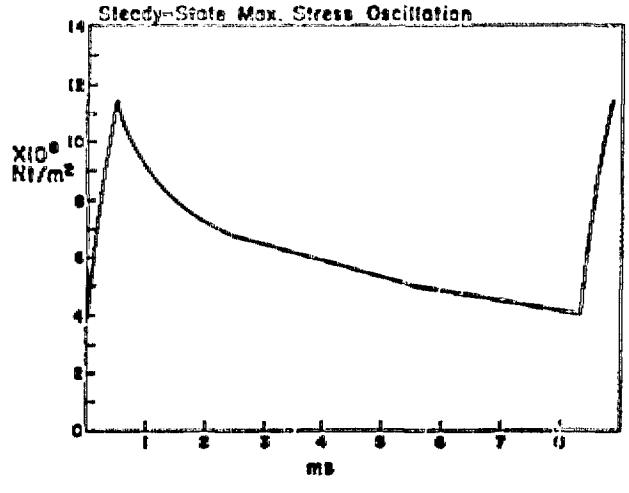

Fig. 11.
Maximum stress during the n + 1 pulse (n → ∞).

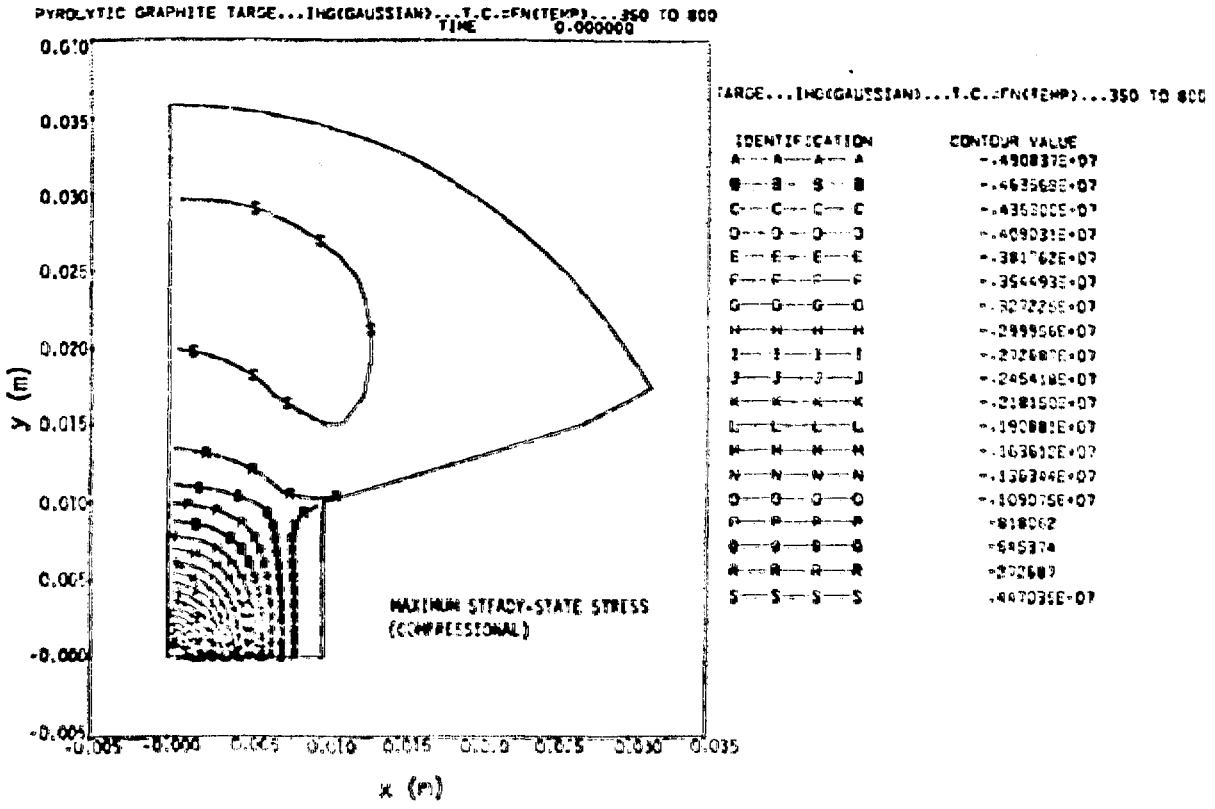

Fig. 12(a).

Maximum steady-state compressional stresses (minus sign indicates compressional stresses) (pascals).

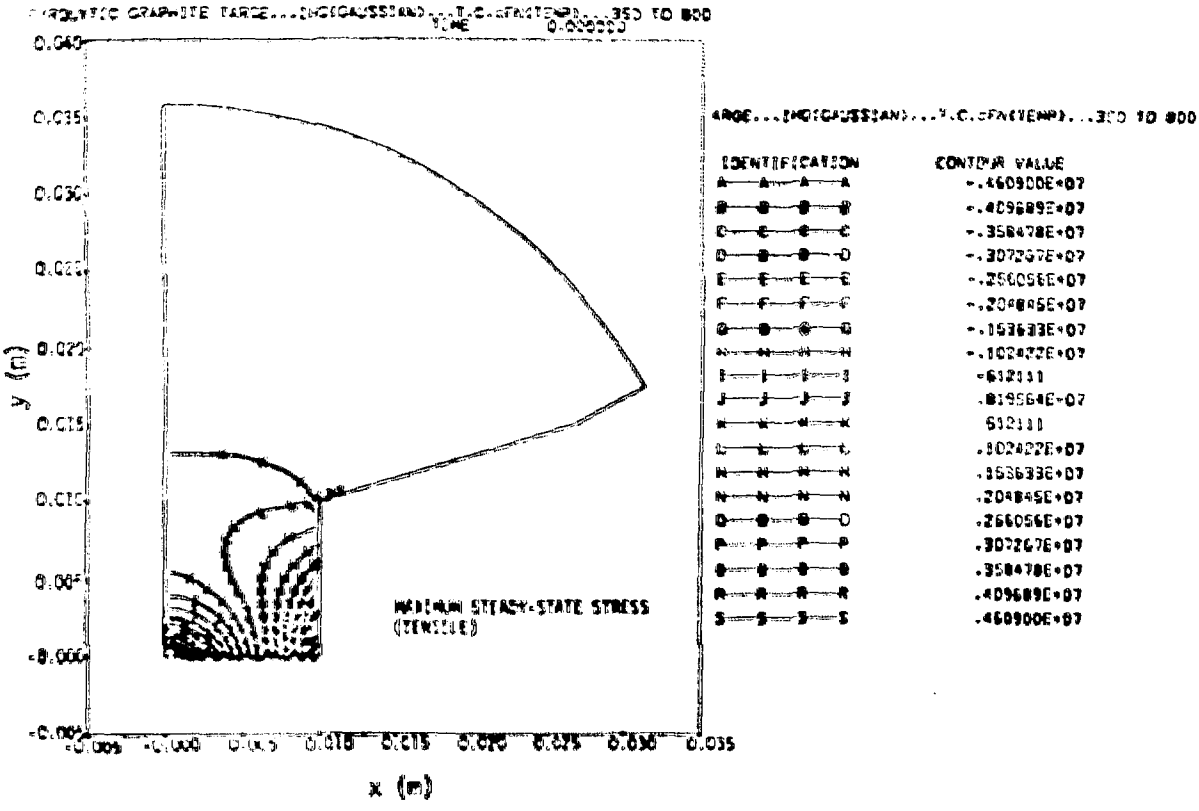

Fig. 12(b).
Maximum steady-state tensile stresses (positive sign indicates tensile stresses).

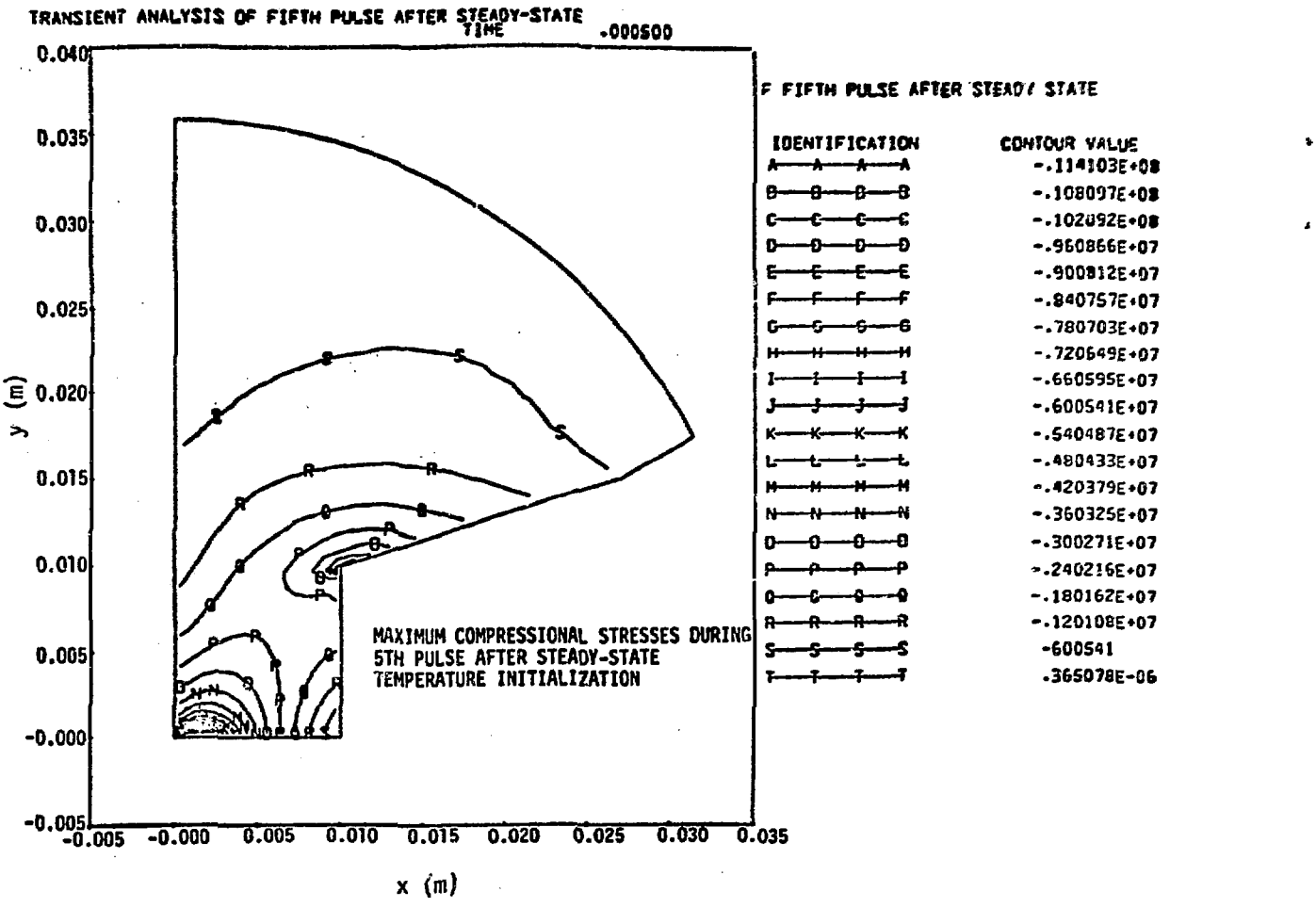

Fig. 13(a).
Maximum compressional stresses during n + 1 pulse (n → ∞).

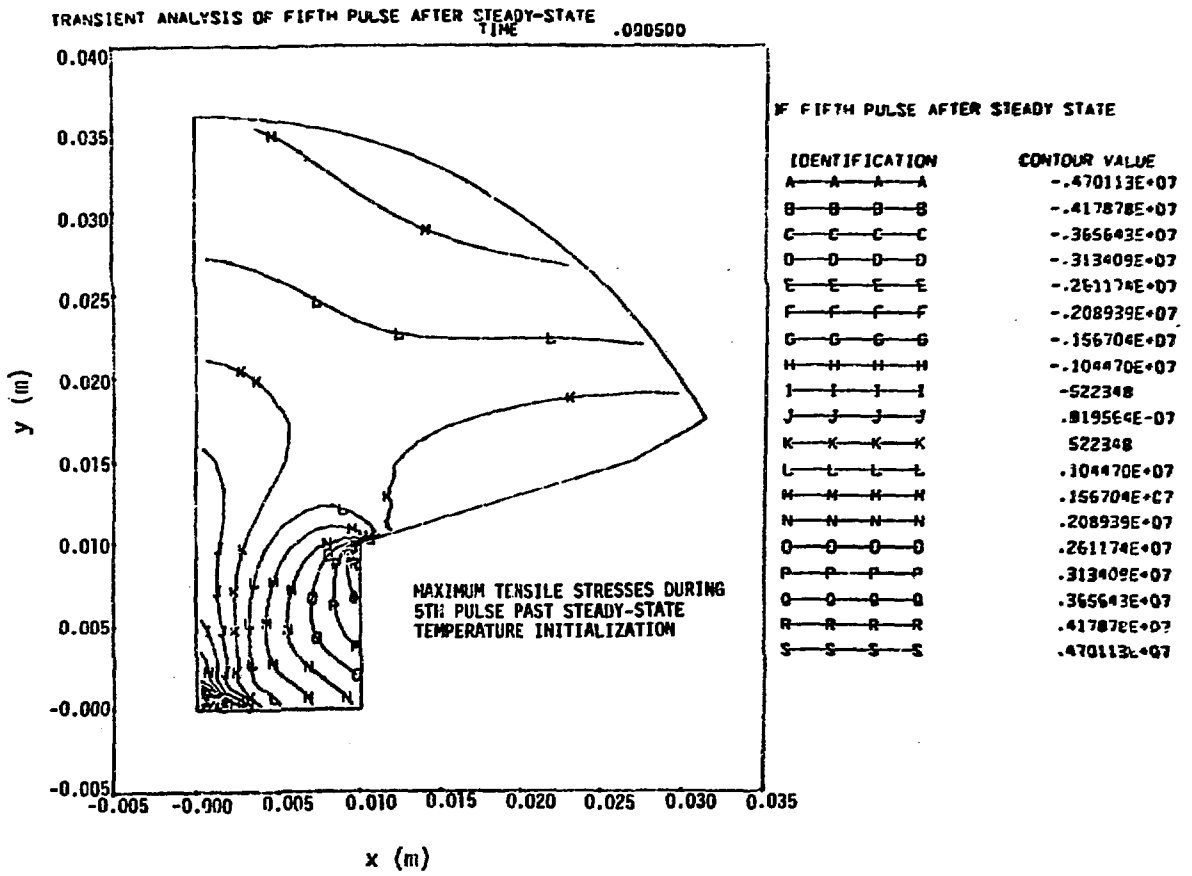

Fig. 13(b).
Maximum tensile stresses during the n + 1 pulse (n → ∞).